Applied Engineering
2023; 7(1): 1-10
http://www.sciencepublishinggroup.com/j/ae
doi: 10.11648/j.ae.20230701.11

Numerical Simulation of Heat and Moisture Transfer in Corrugated Walls Dryer

Balbine Matuam[1, 2, *], Nicolas Gnepie[1], Jaures Fotsa[1], Abraham Tetang[1], Marcel Edoun[1, 2], Et Alexis Kuitche[1]

[1]Applied Energy and Thermal Laboratory (LETA)/National School of Agro-Industrial Sciences (ENSAI), University of Ngaoundere, Ngaoundere, Cameroon

[2]Energy Systems Analysis Laboratory (LASE), University Institute of Technology of Ngaoundere (IUT), Ngaoundere, Cameroon

Email address:

balbinematuam@yahoo.fr (Balbine Matuam)

[*]Corresponding author

To cite this article:

Balbine Matuam, Nicolas Gnepie, Jaures Fotsa, Abraham Tetang, Marcel Edoun, Et Alexis Kuitche. Numerical Simulation of Heat and Moisture Transfer in Corrugated Walls Dryer. *Applied Engineering*. Vol. 7, No. 1, 2023, pp. 1-10. doi: 10.11648/j.ae.20230701.11

Received: January 27, 2023; **Accepted**: February 17, 2023; **Published**: February 28, 2023

Abstract: The primary goal of the current work is to model heat and mass transfer during mango drying in a wavy airflow dryer. By modifying the dryer walls, we were able to produce the undulating airflow (with V-shaped obstacles). With convective boundary conditions applied to all product surfaces, the explicit finite difference approach was used to study heat and mass exchanges in two dimensions during the drying of mango slices. During drying, the transfer coefficients are thought to fluctuate. Using EasyCFD software, the external flow, temperature, velocity, and pressure fields were then analyzed. This provided the profile of the heat transfer coefficient. These profiles were then utilized to calculate the mass transfer coefficient using the Shilton-Colburn analogy. Moreover, the code created to determine the heat and mass transfer coefficients in the product was used to derive the evolution of temperature and moisture content over time. The results allowed for the discovery of a new air flow in dryers called an undular flow and demonstrated how modifying the drying air stream enhanced heat transfer efficiency. By changing the air flow in the dryer, it was possible to achieve heat transfer coefficients ranging from 47.55 W/m^{2}K to 357.38 W/m^{2}K and mass transfer coefficients of 3.21 x 10-5 to 3.21 x 10-4 m^2/s. When the outcomes of this investigation were compared to experimental results from the literature (under identical drying circumstances), a reasonable level of adequacy was discovered.

Keywords: Numerical Simulation, Drying, Dryer, Corrugated Walls, Convective Coefficients

1. Introduction

Drying is a complex process that involves simultaneous heat and mass transfer phenomena inside the product as well as physical or chemical transformations that may affect the product's quality, which is why it requires a lot of energy. 10-15% of all industrial energy use worldwide is accounted for by this expensive and energy-intensive procedure [14]. Due to this significant share, it is essential to determine methods of process optimization that are both affordable and environmentally sustainable. Water that is initially in a liquid form vaporizes throughout the drying process, heating the initially wet product. Heat can be supplied by convection (direct dryers), by conduction (contact dryers or indirect dryers), or by radiation.

Conduction, convection, and radiation are the three mechanisms through which heat is transferred during drying. Convective heat transfer, however, is the main factor in drying agricultural products. The heat transfer coefficient, which measures the barrier to heat and mass transfer between the drying air and the product surface, is a crucial factor in drying simulations [22]. To predict and assess the dryer's thermal performance, you must be aware of this coefficient. As a result, research on heat and mass transport during the drying of porous media has been a focus of both theoretical and experimental effort for many authors for a number of years.

Numerous studies have focused on determining the convective heat transfer coefficient of products during drying. The study of Mahesh et al. was about how forced and natural drying affect the heat transfer coefficient [17]. They demonstrate how it fluctuates significantly depending on the drying method (natural or forced convection). Akpinar [1]

uses a straightforward approach to calculate the convective coefficient (hc) of different products and demonstrates how it is influenced by factors like porosity, moisture content, size, shape, thermophysical properties, and experimental settings. Dragiša et al. [6] assess the impact of heat transfer in a convective air transport dryer and demonstrate, following application to corn, how the heat transfer coefficient depends on the following parameters: heat flux, drying area, and temperature gradient. Anwar and Singh [2] analyze the behavior of the heat transfer coefficient in a laboratory scale dryer by drying currants (fruit with a high moisture content of 80–82%), in 3 different shapes (shredded, sliced, and pieces). They demonstrate that when the product dries, the heat transfer coefficient drops (due to the decrease in moisture content with time). Additionally, they demonstrate that for thin layers, it depends on the product's surface, while for thick layers, it depends on the product's volume. Thus, they reach the conclusion that the transfer coefficient depends on both the product's shape and the drying method.

Most of the publications mentioned above assume that the heat and mass transfer coefficients are constant, concentrating primarily on the internal transport phenomena of temperature and moisture content. These coefficients do, in fact, fluctuate along the surface depending on the temperature field and the external flow.

The analysis of the drying air flow and the coupling of heat and mass transfer in the product have both been taken into consideration in studies. A 2-D numerical model of heat and mass transport during convective flow drying of a rectangular and cylindrical wet object was created by Kaya et al. [11-13]. The equations for heat and mass transfer were solved by a finite difference computational code. They show the optimal ratio for efficient heat transfer and good drying. Hussein and Dincer [9] conduct a 2-D analysis of heat and mass transfer during the drying of a wet cylindrical object. They develop a profile of temperature and moisture content using the explicit finite difference method. In order to resolve the transfer equations during the drying of tropical fruits, Azharul and Hawlader [3] constructed a mathematical model. The product's distortion is taken into consideration by the model. The model estimates the air moisture content and temperature at each location in the tunnel and describes the transfer phenomena in the tunnel dryer. A 1-D mathematical model of simultaneous heat and mass transfer is proposed by Wang and Brennan [26]. They employ the finite difference approach (Crank-Nicolson). A 3-D numerical model was created by Chandra and Talukdar [5] to estimate the transient temperature and moisture distribution during the convective lick flow drying of a rectangular object. The equations governing the concurrent transient heat and mass transfers are solved using a computational code developed using the finite volume method. To investigate the impact of heat and mass transfer on the convective flow-through drying of rubber sheets in an electric dryer, Tekasakul created a 3D numerical model [23]. A two-dimensional analysis of heat and mass transfer during the drying of a square cylinder is carried out by Korukcu [15]. He assesses the moisture content distributions inside the square cylinder using the ADI approach.

These studies assess the heat transfer coefficient of equipment with smooth walls. Although it enhances the drying process and the heat transfer coefficient, it does not completely resolve the issue of drying's energy consumption.

On the other hand, methods to raise the heat transfer coefficient by modifying the air stream are mentioned in other works on pipes and heat exchangers. The following are works by:

Ray and Date [20] performed a numerical analysis of the heat transfer via a square pipe with a worm-shaped rod moving in laminar flow. Following investigation, it was determined that the rod improved heat transfer. Additionally, they demonstrate that, for the identical conditions, a square pipe increases heat transmission more than a circular pipe. According to the work of Jawarneh [10], the vortex effect is used to boost heat transfer, especially if the number of rotations is significant. The increase in heat transfer in a corrugated tube with a helical ribbon added is examined by Eiamsa-ard and Promvonge [7]. They demonstrate that compared to a straightforward corrugated surface, the corrugated tube with helical ribbon provides an increase in heat transfer rate and friction factor of roughly 57%. According to this research, altering the air flow can greatly raise the heat transfer coefficient. However, numerous dryer-related experiments have not produced these outcomes.

Therefore, the purpose of the current work is to emphasize the impact of changing the air flow on the heat transfer coefficient between the air and the product. It is necessary to evaluate and predict the distributions of temperature, air velocity, and pressure inside the dryer and around the product by numerically analyzing the behavior of the convective coefficient of heat when obstacles are added to a dryer (with corrugated walls) with licking flow to cause an undulatory displacement of the air.

To achieve this, we'll:

1) Utilize the EasyCFD program to analyze the external flow and temperature field.
2) Identify the space-dependent heat transfer coefficient (X, Y).
3) Apply the thermal and concentration layer analogies to get the mass transfer coefficient at each location.
4) Using the explicit finite difference method, calculate the product's temperature and moisture content distribution,
5) and compare the results to the model developed by Matuam et al. [18] for their experimental drying.

2. Mathematical Modeling

2.1. Air Flow Modeling in the Drying Sector

The physical model under investigation is shown in figure 1. It is a rectangular chamber (dryer) with dimensions of H in height and L in length where the products (with a moisture content of M) are placed. The dryer's upper and bottom walls are covered in triangular-shaped obstructions that are evenly

spaced throughout the surfaces. Hot air is introduced to the products in a licking flow at speed V. The horizontal walls are maintained to be impermeable and adiabatically (Neumann conditions). The final outcome is an initial slice of mango with a thickness of e, an initial air temperature of T_0, and an initial moisture content of M_0. Only the product's bottom and top surfaces are thought to benefit from drying. The product's surface comes into contact with the drying air. The temperature of the air is constant.

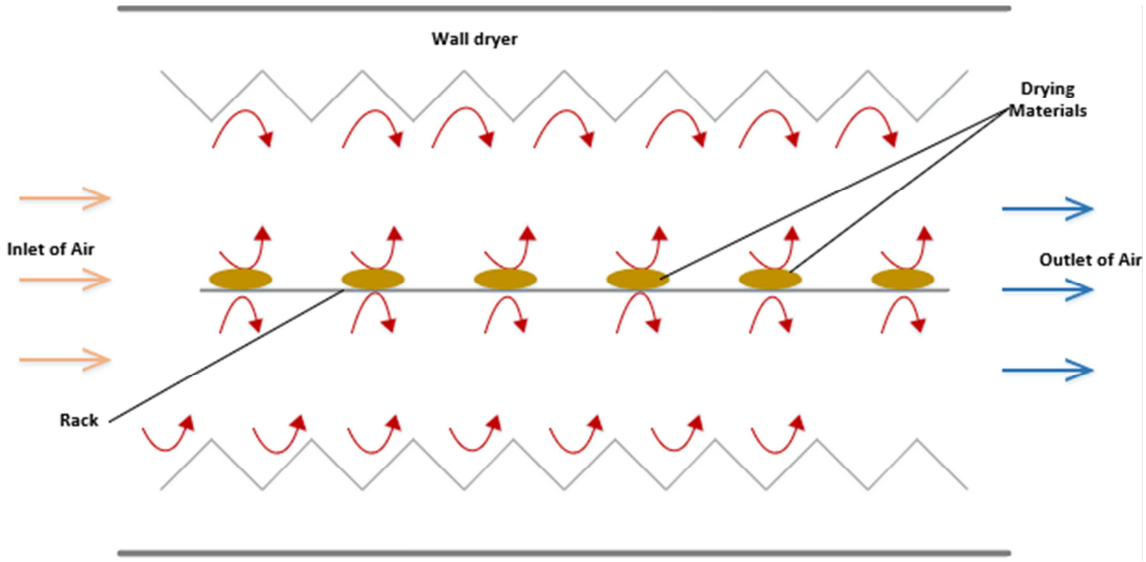

Figure 1. *Product dried by convection.*

The mass, momentum, and energy conservation equations only apply to the bottom and top faces of the product when controlling the forced convective motion of a drying fluid in a 2-D geometry. For the purpose of describing the turbulent flow, the *K*-ε model is used. The thermo-physical properties are taken to remain constant in order to simplify the issue (i.e., the variation of the fluid properties with temperature is neglected). The Navier-Stockes equations are given in their most generic form when the incompressible flow is taken into account.

2.1.1. Continuity Equation

$$\frac{\partial(\rho u)}{\partial x}+\frac{\partial(\rho v)}{\partial y}=0 \quad (1)$$

where u and v are velocity components, and ρ is volumic mass.

2.1.2. Momentum Equation

According to the axial direction:

$$\rho\left(u\frac{\partial u}{\partial x}+v\frac{\partial u}{\partial y}\right)=\beta-\frac{\partial P^*}{\partial x}+(\mu+\mu_t)\left(\frac{\partial^2 u}{\partial x^2}+\frac{\partial^2 u}{\partial y^2}\right) \quad (2)$$

According to the radial direction:

$$\rho\left(u\frac{\partial v}{\partial x}+v\frac{\partial v}{\partial y}\right)=-\frac{\partial P^*}{\partial y}+(\mu+\mu_t)\left(\frac{\partial^2 v}{\partial x^2}+\frac{\partial^2 v}{\partial y^2}\right) \quad (3)$$

2.1.3. Energy Equation

$$\rho C_P\left(u\frac{\partial \hat{T}}{\partial x}+v\frac{\partial \hat{T}}{\partial y}\right)=\left(\frac{\mu}{Pr}+\frac{\mu_t}{Pr_t}\right)\left(\frac{\partial^2 \hat{T}}{\partial x^2}+\frac{\partial^2 \hat{T}}{\partial y^2}\right)-\rho C_P\sigma u \quad (4)$$

where μ (N s/m^2) is the dynamic viscosity, and μ_t the turbulent viscosity.

2.1.4. Turbulent Kinetic Energy Equation

$$\frac{\partial(\rho uk)}{\partial x}+\frac{\partial(\rho vk)}{\partial y}=\frac{\partial}{\partial x}\left[\left(\mu+\frac{\mu_t}{\sigma_k}\right)\frac{\partial k}{\partial x}\right]+\frac{\partial}{\partial y}\left[\left(\mu+\frac{\mu_t}{\sigma_k}\right)\frac{\partial k}{\partial y}\right]+P_k-\rho\varepsilon+G_T \quad (5)$$

2.1.5. Dissipation Rate Equation

$$\frac{\partial(\rho u\varepsilon)}{\partial x}+\frac{\partial(\rho v\varepsilon)}{\partial y}=\frac{\partial}{\partial x}\left[\left(\mu+\frac{\mu_t}{\sigma_\varepsilon}\right)\frac{\partial \varepsilon}{\partial x}\right]+\frac{\partial}{\partial y}\left[\left(\mu+\frac{\mu_t}{\sigma_\varepsilon}\right)\frac{\partial \varepsilon}{\partial y}\right]+C_1\frac{\varepsilon}{k}P_k-C_2\rho\varepsilon+C_3G_T \quad (6)$$

$$P_k=\mu_t[2\left(\frac{\partial u}{\partial x}\right)^2+2\left(\frac{\partial v}{\partial y}\right)^2+2\left(\frac{\partial u}{\partial y}+\frac{\partial v}{\partial x}\right)^2] \quad (7)$$

$$G_T=-\beta g\frac{\mu_t}{Pr_t}\frac{\partial T}{\partial y} \quad (8)$$

with: $C_\mu=0{,}09\ \sigma_k=1{,}0\ \sigma_\varepsilon=1{,}3\ C_1=1{,}44\ C_2=1{,}92\ C_3=1{,}44$

The creation of a periodic flow is induced by the presence of baffles in the pipe, and this results in the periodic behavior of temperature and pressure that is represented as follows:

$$P(x,y)=-\beta x+P^*(x,y)\ \ [24] \quad (9)$$

with:

$$\beta=\frac{\Delta p}{2H} \quad (10)$$

where: β = Average pressure along the horizontal axis

P^* = New pressure in the pipe

$$T(x,y)=\sigma x+T^*(x,y) \quad (11)$$

with:

$$\sigma = \frac{2q_0}{\rho \bar{u} C_P D} \quad (12)$$

Where: σ = Average temperature along the horizontal axis

T^* = New Temperature in the pipe

The turbulent viscosity μt is calculated from the k-ε turbulence model.

The EasyCFD software, which is based on the finite volume approach, was used to solve these equations. The pressure-velocity coupling issue was resolved using the SIMPLEC algorithm. The local heat transfer coefficient is determined using the temperature fields that were acquired by:

$$-k\frac{\partial T}{\partial n} = h\,(T_s - T_m) \quad (13)$$

where n is the surface normal vector s and Tm the mean wet temperature.

The Chilton-Colburn analogy is used to compute the mass transfer coefficient hm after determining the heat transfer coefficient h.

$$h_m = h(\frac{DLe^n}{k}) \quad (14)$$

with*:* h: Heat transfer coefficient (W/m^{2}K)

D: Mass diffusivity (m^2/s)

k: Thermal conductivity (W/m. K)

Le: (= α/D) is the Lewis number representing a relative measure of the thermal and concentration boundary layer thickness and for most applications n is taken as 1/3 [5].

2.2. Modeling the Internal Temperature and Moisture Fields of the Product

The following simplifying assumptions were made in order to analyze the heat and mass transfer: The transfers are one-dimensional. The deformation of the product during drying is neglected. The physical properties of the product are constant; the thermo-physical properties of the air are constant; the radiative exchanges inside the enclosure are neglected; the convective exchanges between the air and the walls of the climate enclosure are neglected; the temperature and water content are initially uniform in the product; the heat generated inside the product is neglected.

The equations governing the convective transfers in 2-D are written as follows:

$$\frac{1}{\alpha}\frac{\partial T}{\partial t} = \frac{\partial^2 T}{\partial X^2} + \frac{\partial^2 T}{\partial Y^2} \quad (15)$$

$$\frac{1}{D}\frac{\partial M}{\partial t} = \frac{\partial^2 M}{\partial X^2} + \frac{\partial^2 M}{\partial Y^2} \quad (16)$$

The initial conditions are:

T (x, y, t) =T (x, y,0) =Ts et M (x, y, t) = M (x, y, 0) = Ms

The boundary conditions are:

at x = 0; 0 ≤ y ≤ b,

$$-K\,\frac{\partial T(0,y,t)}{\partial x} = h(T - T_{air});$$

$$-D\,\frac{\partial M\,(0,y,t)}{\partial x} = h_m\,(M - M_{air})$$

at x = a; 0 ≤ y ≤ b

$$-K\,\frac{\partial T(a,y,t)}{\partial x} = h(T - T_{air});$$

$$-D\,\frac{\partial M\,(a,y,t)}{\partial x} = h_m\,(M - M_{air})$$

at y = 0; 0 ≤ x ≤ a

$$-K\,\frac{\partial T(x,0,t)}{\partial y} = h(T - T_{air});$$

$$-D\,\frac{\partial M\,(x,0,t)}{\partial y} = h_m\,(M - M_{air})$$

at y = b; 0 ≤ x ≤ a

$$-K\,\frac{\partial T(x,b,t)}{\partial y} = h(T - T_{air});$$

$$-D\,\frac{\partial M\,(x,b,t)}{\partial y} = h_m\,(M - M_{air})$$

With *D: mass diffusivity coefficient (m^2/s); et α: Thermal diffusivity (m^2/s),*

M: Moisture content;

Where D is obtained from the Arrhenius equation

$$\mathrm{D} = \mathrm{D_0}\exp(-\frac{\mathrm{E_a}}{\mathrm{R(T+273,15)}}) \quad (17)$$

with the Arrhenius factor D_0 equal to 3.28 x 10-7 m^2/s. The product is assumed to have a constant surface temperature of 25°C and an initial moisture content of 90%.

A computation code was created in the Matlab environment utilizing the explicit finite difference discretization method. The stability criterion of these equations is

for mass transfer:

$$\Delta t \leq \frac{1}{2D}\frac{\Delta x^2 \times \Delta y^2}{((\Delta x^2)+(\Delta y^2))} \quad (18)$$

for heat transfer:

$$\Delta t \leq \frac{1}{2\alpha}\frac{\Delta x^2 \times \Delta y^2}{((\Delta x^2)+(\Delta y^2))} \quad (19)$$

The iterative Gauss-Seidel method was used to solve the resulting equations. Simultaneously, the mass and heat transfer equations were solved. When conditions (18) and (19) are satisfied, the convergent point is reached.

3. Results and Discussion

3.1. Airflow Simulation

The simulations were performed for air inlet temperatures of 40°C, 50°C, and 60°C and for velocities of 0.5 m/s, 1 m/s, and 2 m/s. The aim of the CFD simulation is to assess the heat transfer coefficient on the surface of the product that has been

placed in the dryer. It is independent of the dryer inlet temperature. The simulation parameters are taken from the work of Matuam et al. [18]. Only one case is provided here because all velocity and temperature cases have the same tendencies in velocity, temperature, and pressure contours.

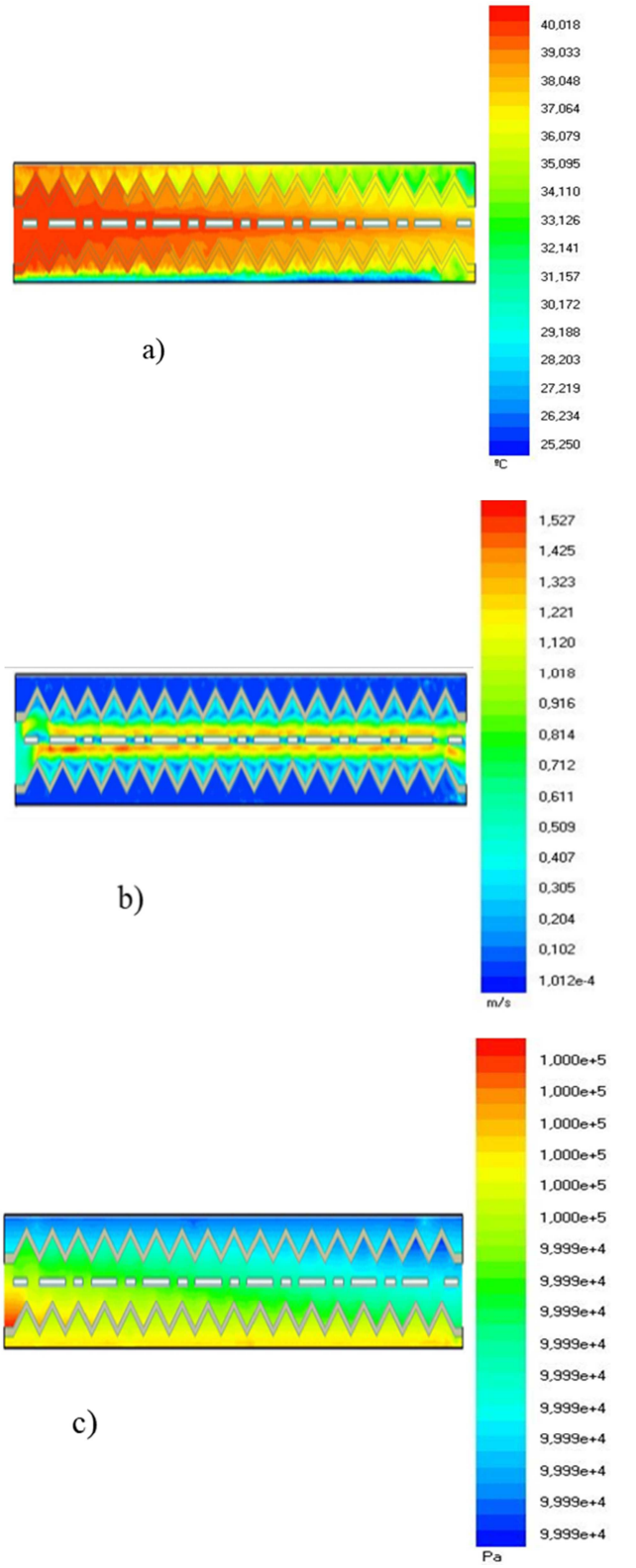

Figure 2. *(a) Temperature field, (b) velocity field, (c) pressure field around the products (40°C; 0.5 m/s).*

Figure 2 shows the pressure (c), velocity (b), and temperature (a) fields, respectively, along the dryer and surrounding the products. The temperature along the pipe in figure 2 (a) is seen to have decreased by around 3°C as a result of the pipe's length and the presence of obstructions on its walls, respectively. Additionally, a temperature increase is seen in the pipe's middle or around the products. The range of temperatures is 40 to 37°C. Figure 2 (b) illustrates how the velocity rises along the pipe as the concentration increases closer to the products. The speed changes from 0.5 m/s to 1.5 m/s. Figure 2 (b) illustrates how the velocity rises along the pipe as the concentration increases closer to the products. Variations in velocity range from 0.5 to 1.5 m/s. This may be caused by the baffles and the products, which double the amount of air that is dissipated. This would also explain the pressure's behavior, which is high at the entry and significantly lower along the dryer (Figure 2 (c)).

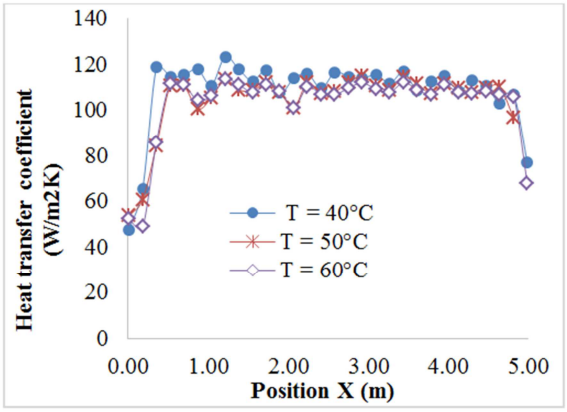

a)

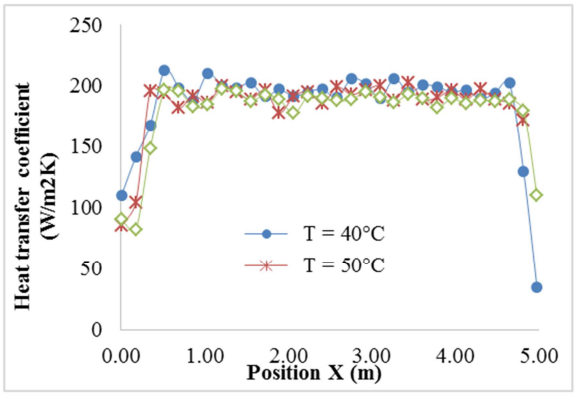

b)

Figure 3. *Heat transfer coefficient as a function of temperature at 0.5 m/s (a) and 1 m/s (b).*

Figure 3 depicts the distribution of the heat transfer coefficient at velocities of 0.5 m/s and 1 m/s at the surface facing the air inlet. The heat transfer coefficient exhibits a very slight temperature-dependent change. This may be due to linear and singular losses in the channel. Additionally, we see that the heat transfer coefficient changes in a sawtooth pattern, which is probably caused by the arrangement of barriers on the air flow channel's walls. We can describe it as an undulating flow as a result.

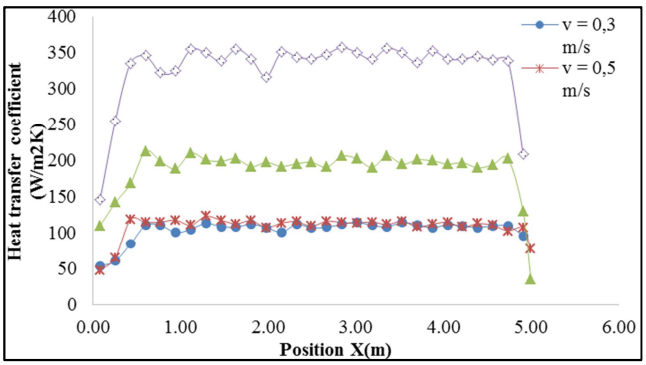

Figure 4. *Heat transfer coefficient at 40°C as a function of speed.*

Figure 4 illustrates how the increase in air inlet affects the behavior of the heat transfer coefficient at the boundary facing the channel inlet. It is clear that an increase in airflow velocity causes the heat transfer coefficient to increase practically proportionally because of the greater convection that results from the higher airflow. Due to a homogenous incoming flow, the change in the heat transfer coefficient displays a symmetrical distribution. This conclusion is comparable to that made on smooth walls by Chandra and Talukdar [5].

Figures 3 and 4 show a transfer coefficient that rises rapidly at the start of the drying process (due to the temperature differential), holds steady throughout the process, and falls at the conclusion (most of the water contained in the product has disappeared, the product has shrunk, thus obstructing the pores; this no longer favors the passage of heat).

The significant outcomes of heat and mass transmission in terms of minimum and maximum are summarized in Table 1 below. This makes it possible to present and comprehend the drying phenomenon better. For varied velocities and temperatures, the values of the heat transfer coefficient range from 47.55 to 357.38 W/m^{2}K, while those of mass transfer range from 3.21E-05 to 3.21E-04 m^2/s.

Table 1. *Minimum and maximum values of convective transfer coefficients.*

	Heat (W/m^{2}K) and mass (m^2/s) transfer coefficients								
	0,5 m/s			**1 m/s**			**2 m/s**		
	Min	**Max**	**Moy**	**Min**	**Max**	**Moy**	**Min**	**Max**	**Moy**
40°C									
hc	47.55	118.56	108.39	35.02	212.70	184.70	146.59	357.38	328.76
hm	3.21E-05	8.31E-05	7.31E-05	7.45E-05	1.43E-04	1.25E-04	9.88E-05	2.41E-04	2.22E-04
50°C									
hc	53.73	114.87	104.52	86.14	202.94	185.08	143.65	352.56	324.51
hm	4.34E-05	9.27E-05	8.43E-05	6.95E-05	1.64E-04	1.49E-04	1.16E-04	2.84E-04	2.62E-04
60°C									
hc	48.85	113.50	102.59	82.74	197.40	178.50	172.03	342.60	310.60
hm	4.49E-05	7.87E-05	7.16E-05	7.60E-05	1.81E-04	1.64E-04	1.58E-04	3.21E-04	2.85E-04

Figure 5 depicts the distribution of mass transfer on the product face in close proximity to the air inlet. The fact that the heat transfer coefficient is calculated using the Chilton-Colburn analogy can be used to explain why it has the same shape as this curve. Furthermore, when the temperature changes, the mass transfer coefficient changes very little.

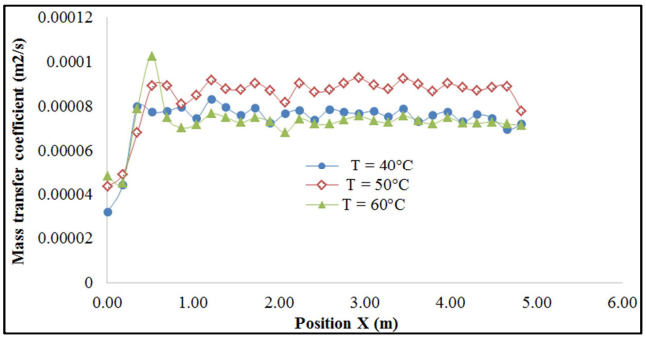

Figure 5. *Mass transfer coefficient as a function of temperature at 0.5 m/s.*

The behavior of the mass transfer coefficient as the air inlet velocity varies is depicted in Figure 6. These curves resemble those of the heat transfer coefficient in appearance (Figures 3 and 4). The convective transfer coefficient increases quickly at the boundary facing the entrance as a result of direct contact with the hot air, as seen in Figures 3, 4, 5, and 6. The transfer coefficient rises, develops in a sawtooth pattern, and then steadily declines to its minimal value.

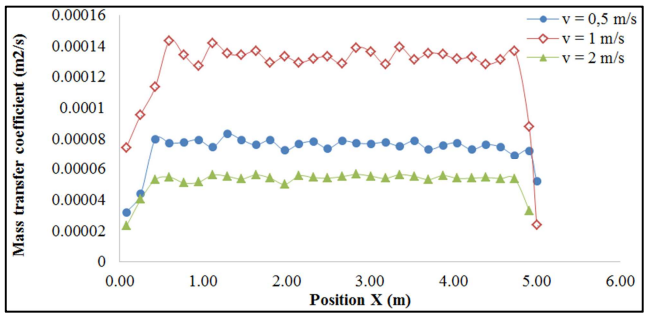

Figure 6. *Coefficient de transfert de masse en fonction de la température à 40°C.*

On the other hand, because of decreased exposure to warm air, convective transfer coefficients are low near the border facing the outlet. Mass transfer is enhanced by the increase in velocity. On smooth walls, Kaya et al. [11] found comparable findings.

Figure 7 demonstrates that the progression of the friction factor in the pipe is unaffected by temperature. There are three very identical curves in this illustration. The curves

reveal an initial peak (corresponding to the entry of air into the pipe) and a stable curve throughout the pipe. Low pressure drop measurements are noted along the flow.

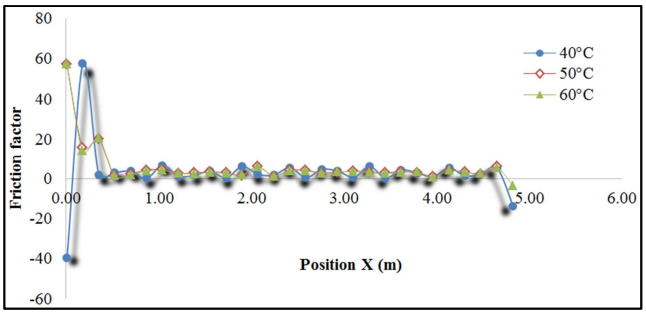

Figure 7. *Evolution of the friction factor.*

3.2. Modeling of Convective Transfers

The evolution of temperature and water content in the product is evaluated at several instants using a computational code in the Matlab environment that was developed by the authors. For this purpose, the heat and mass transfer coefficients obtained previously from the external flow study were used. The parameters used here are listed in Table 2.

Table 2. *Simulation parameters ([21, 27]).*

Parameters	Symbol	Value	Unity
Product density	ρ	1033	kg/m^3
Specific heat	C_p	3726	$J/kg.K^{-1}$
Thermal conductivity	K	0.4398	$W/m.K^{-1}$
Diffusivity	D_{eff}	Present work	m^2/s
Latent heat of vaporization	L_v	2.345×10^3	kJ/kg
Initial temperature	T_0	40	°C
Initial water content	M_0	0.9	kg/kg of mater
Heat transfer coefficient	h	Present work	$W/m^2 K$
Mass transfer coefficient	h_m	Present work	m^2/s

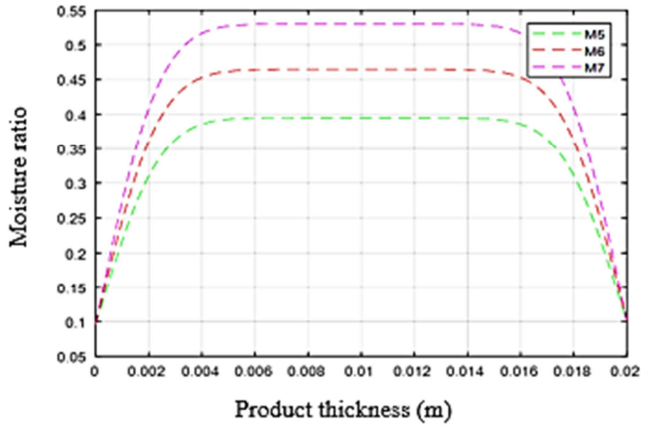

Figure 8. *Evolution of the moisture ratio as a function of the thickness of the product for a position (x, y).*

Figure 8 represents the internal profile of the product's water content for a specific place (x, y) at a specific period. We have the curves of figure 8 at the locations denoting the times 5h (M5), 6h (M6), and 7h (M7). The distribution of water in the sample is depicted in this image as a function of both position and drying time during drying at 40°C. While the moisture content near the sample's bottom steadily drops with drying time, the gradients in moisture content from the sample's surface to its bottom decrease as drying time increases. This outcome is comparable to that described in the drying theories by the authors [19, 25, 26].

Figure 9 illustrates the sample's anticipated temperature distribution as a function of position and 40°C drying time. It is evident that when the product dries, the temperature rises at every location. With longer drying times, the temperature differences between the product's surface and bottom are reduced. The same outcomes were reached by Wang and Brennan [26].

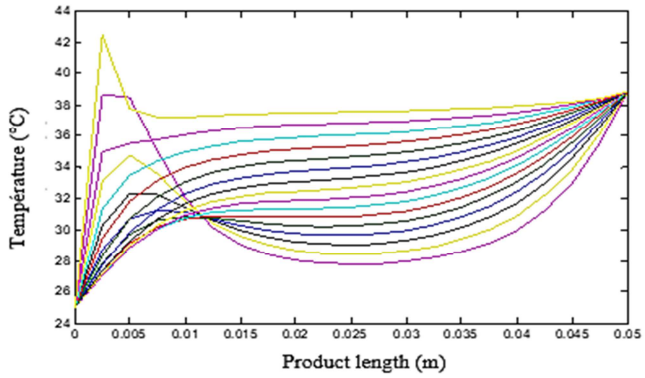

Figure 9. *Evolution of product temperature as a function of thickness for a position (x, y).*

At 40°C and 0.5 m/s, Figure 10 depicts the effect of product mass on moisture ratio (10a) and temperature (10b) as a function of time. Figure 10a shows the moisture ratio evaporating over time. The amount of moisture lost during drying is significantly influenced by the product's mass; the heavier the product, the longer it takes to dry.

At the conclusion of the drying process, the temperature has reached the predetermined degree after gradually rising during the procedure (10b). The same outcomes were attained by Bennamoun et al. [4]. Additionally, the density of the product affects how the temperature changes within it. These findings concur with those made by Hemis et al. [8] and Mabrouk et al. [16].

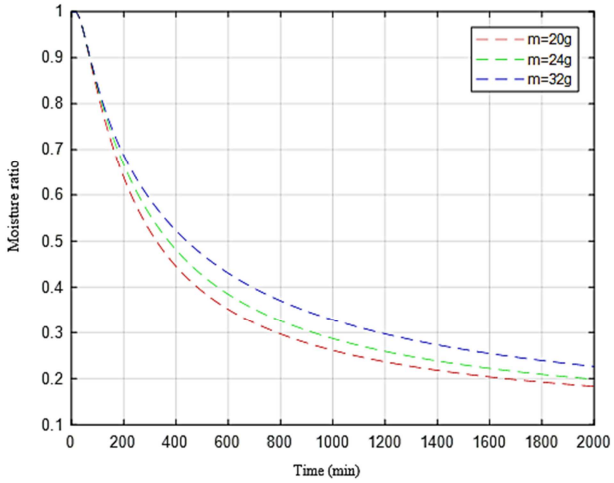

a)

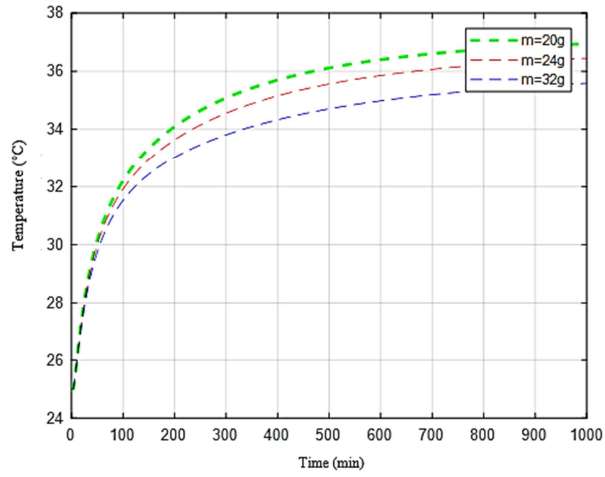

b)

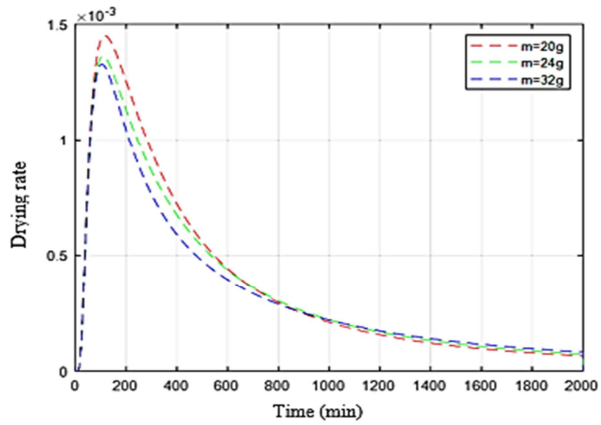

c)

Figure 10. *Influence of product mass on moisture ratio (a), temperature (b) and drying rate (c).*

Figure 11 compares the evolution of the reduced moisture ratio over time between the experimental and numerical results for lick flow drying.

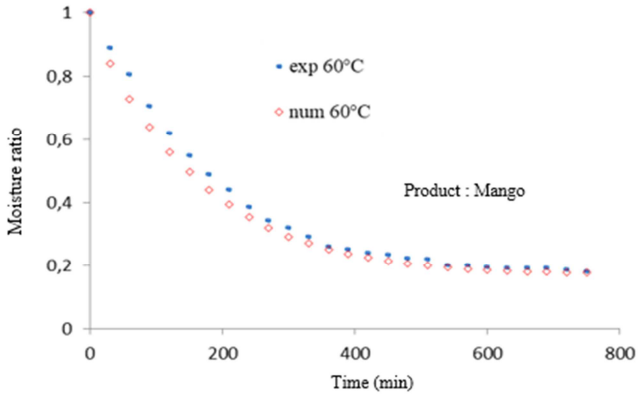

Figure 11. *Comparison between the predicted and calculated value of the moisture ratio distribution in the product.*

Only the moisture ratio distribution is depicted in Figure 11 because the temperature distribution in the product is unavailable. The findings achieved experimentally and those anticipated are shown to be in good agreement in this figure. As a result, the heat and mass transport in the product during drying may be modeled using the numerical approach described above and the created calculation code.

Figure 12 depicts the temperature progression of the product for various heat transfer coefficient values (h). The temperature's relationship to undulations is depicted in this graph. According to the physical model used in this study, the curve (h = cste) reflects the development of temperature in a smooth wall dryer, while the curve (h = var) represents the evolution of temperature in a corrugated wall dryer. The figure reveals that the presence of corrugations promotes faster drying compared to a smooth pipe system. This result confirms the fact that the modification of the air stream by inserting baffles on the walls of the dryer improves heat transfer.

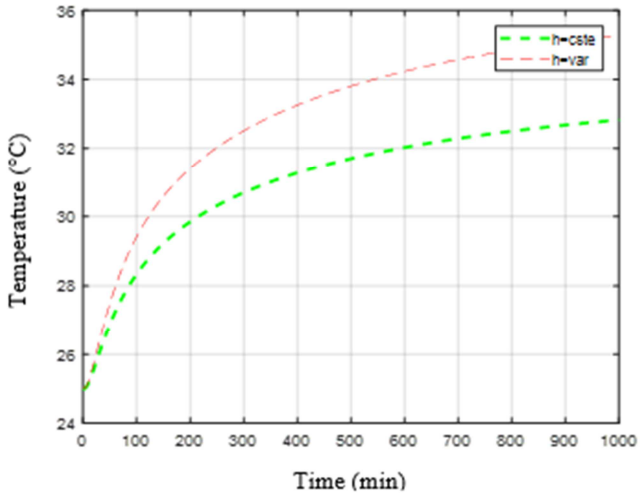

Figure 12. *Influence of undularities on the evolution of the product temperature.*

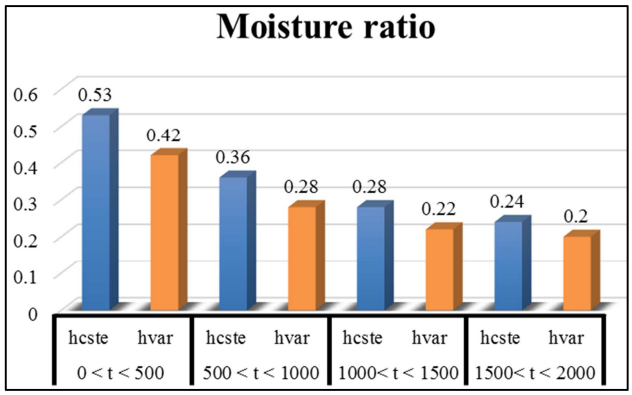

Figure 13. *Comparison of the evolution of the moisture ratio as a function of time.*

In Figure 13, we contrast the changes in the reduced moisture ratio over time in dryers with smooth walls (where the constant heat transfer coefficient is h = cste) and dryers with rough walls (where, in the physical model under consideration, h = var). The target moisture content is attained more quickly during drying thanks to the undulations on the dryer walls, as this figure clearly demonstrates. In fact, the barriers on the dryer's walls encourage an increase in the heat

transfer coefficient, which in turn makes it easier for the hot air and the item to be dried to interact.

Table 3. *Comparison of predicted water content values as a function of time and experimental value.*

Drying time	**0 < t < 500**		**500 < t < 1000**		**1000 < t < 1500**		**1500 < t < 2000**	
Configurations	**hcste**	**hvar**	**hcste**	**hvar**	**hcste**	**hvar**	**hcste**	**hvar**
Moisture ratio	0.53	0.42	0.36	0.28	0.28	0.22	0.24	0.2
Temperature	33.75	39	34	39				

A summary of the moisture content values as a function of drying time in a dryer with smooth walls and one with rough walls is shown in Table 3 above.

4. Conclusion

This work presents the numerical solution of the heat and mass transfer equations occurring inside mango slices as they dry. The dryer being used in this instance has V-shaped barriers on the walls. Analysis was done on the velocity and temperature fields outside. Along the surface of the products, the convective heat transfer coefficient was assessed. The determination of the mass transfer coefficient was then foreseen by comparing the heating and concentrating boundary layers. The results show that the values for the mass transfer coefficient were 3.21E-05 and 3.21E-04 m^2/s, whereas the values for the heat transfer coefficient ranged from 47.55 to 357.38 W/m^2K.

Comparing drying in a dryer with smooth walls to drying in one with corrugated air flow allowed to assess the contribution of the latter. The system without corrugation was initially studied using a programming code, and the system with corrugation was subsequently studied. We plotted the drying kinetics using the generated Matlab code, and they agreed with the drying theories and works in the literature. The validation of our code was prompted by this first outcome. The code additionally allowed us to compare the drying systems with smooth walls and corrugated walls; the corrugated wall system resulted in a gain of 5 hours in drying time.

According to the results, the drying system with corrugation is superior to the drying system with a smooth wall in terms of heat and mass transport. So, drying in a dryer with a rough wall enables the dryer to use less energy. This is an asset for future work on drying.

This result opens a door to the study of air flows in drying. It clearly shows that the researchers, in their quest for improvement of the drying process, will have to take into account the modification of the airflow in a logic of optimization. Moreover, it would be interesting to implement this wave flow in the design of new dryers for experimental studies.

References

[1] Akpinar E. K. (2005). Evaluation of convective heat transfer coefficient of various crops in cyclone type. Energy Conversion and Management. Vol. 46. pp 2439–2454.

[2] Anwar S. I., Singh, R. D. (2012). Convective heat transfer coefficient of Indian gooseberry (emblica officinalis) dried in three different forms under forced convection mode. Journal of Engineering Science and Technology. Vol. 7. No. 5. pp 635 – 645.

[3] Azharul K., Hawlader M. N. A. (2005). Mathematical modelling and experimental investigation of tropical fruits drying. International Journal of Heat and Mass Transfer. Vol 48. pp 4914–4925.

[4] Bennamoun L., Fraikin L., and Leonard A. (2014). Modeling and Simulation of Heat and Mass Transfer During Convective Drying of Waste water Sludge with Introduction of Shrinkage Phenomena. Drying Technology. Vol. 32. pp 13–22.

[5] Chandra Mohan V. P., Talukdar P. (2010). Three-dimensional numerical modeling of simultaneous heat and moisture transfer in a moist object subjected to convective drying. International Journal of Heat and Mass Transfer. Vol. 53. pp 4638–4650.

[6] Dragiša Tolmač, Slavica Prvulović, Ljiljana Radovanović. (2008). Effects of Heat Transfer on Convection Dryer with Pneumatic Transport of Material. FME Transactions. Vol. 36. No 1. pp 45-49.

[7] Eiamsa-ard, S., Promvonge, P. (2007). Enhancement of Heat Transfer in a Circular Wavy-surfaced Tube with a Helical-tape Insert. International Energy Journal. Vol 8. pp 29-36.

[8] Hemis M., Singh B. C., Jayas S. D. and Bettahar A. (2011). Simulation of Coupled Heat and Mass Transfer in Granular Porous Media: Application to the Drying of Wheat. Drying Technology. Vol. 29. pp 1267–127.

[9] Hussein M., Dincer I. (2003). Two-dimensional heat and moisture transfer analysis of a cylindrical moist object subjected to drying: A finite-difference approach. International Journal of Heat and Mass Transfer. Vol 46. pp 4033–4039.

[10] Jawarneh Ali M. (2007). Heat Transfer Enhancement in Swirl Annulus Flows. 5th Wseas Int. Conf. On Environment, Ecosystems and Development, Tenerife, Spain. December pp 14-16.

[11] Kaya A., Aydın O., Dincer I. (2006). Numerical modeling of heat and mass transfer during forced convection drying of rectangular moist objects. International Journal of Heat and Mass Transfer. Vol. 49. pp 3094–3103.

[12] Kaya A. and Aydin O., Dincer I. (2007). Numerical Modeling of Forced-Convection drying Of Cylindrical Moist Objects. Numerical Heat Transfer, Part A. Vol. 51. pp 843–854.

[13] Kaya A., Aydın O., Dincer I. (2008). Experimental and numerical investigation of heat and mass transfer during drying of Hayward kiwi fruits (Actinidia Deliciosa Planch). Journal of Food Engineering. Vol. 88. pp 323–330.

[14] Khaldi. (2018). Etude numérique du comportement thermique d'un séchoir solaire utilisant un lit thermique pour le stockage d'énergie. Thèse soutenue en vue de l'obtention du Doctorat de l'Université Bourgogne Franche-Comte.

[15] Korukcu, M. O. (2017). Numerical Modeling of Heat and Mass Transfer Characteristics During the Forced Convection Drying of a Square Cylinder Under Strong Blockage. Numerical Heat Transfer, Part A: Applications. Vol. 72. No 2. pp 171–184.

[16] Mabrouk B. S., Benalia E., Oueslatia H. (2012). Experimental Study and Numerical Modelling of Drying Characteristics of Apple Slices. Food And Bio Products Processing. Vol. 90. pp 719–728.

[17] Mahesh Kumar, Pankaj Khatak, Ravinder Kumar Sahdev. (2011). The effect of open sun and indoor forced convection on heat transfer coefficients for the drying of papad. Journal of Energy in Southern Africa. Vol. 22. No 2.

[18] Matuam B., Edoun M., Kuitche A., Zeghmati B. (2015). Experimental Evaluation of the Thermal Performance of Dryer Airflow Configuration. International Journal of Energy Engineering. vol 5. N°4. pp 80-86.

[19] Nadeau J. P., Puiggali J. R. (1995). Séchage: des processus physiques aux procédés industriels. Technique et Documentation – Paris: Lavoisier. pp 112-126.

[20] Ray S. et Date A. W. (2001). Laminar flow and heat transfer through square duct with twisted tape insert. International journal of heat and fluid flow. Vol. 22. pp 460-472.

[21] Shahari, N. A. (2012). Mathematical Modeling of Drying Food Products: Application To Tropical Fruits. Thèse soutenue en vue de l'obtention du Doctorat PHD à l'Université de Nottingham.

[22] Talukdar P., IskraC. R., Simonson C. J. (2007). Combined heat and mass transfer for laminar flow of moist air in a 3D rectangular duct: CFD simulation and validation with experimental data. International Journal of Heat and Mass Transfer. Vol. 51. pp 3091–3102.

[23] Tekasakul P., Dejchanchaiwong R., Tirawanichakul Y., and Tirawanichaku S. (2015). Three-Dimensional Numerical Modeling of Heat and Moisture Transfer in Natural Rubber Sheet Drying Process. Drying Technology. Vol. 33. pp 1124–1137.

[24] Utriainen E., Sunden B. (2002). A numerical investigation of primary surface rounded cross wavy ducts. Heat and Mass Transfer. Vol 38. pp 537-542.

[25] Vijayaraj, B., & Saravanan, R. (2008). Numerical Modeling of Moisture and Temperature Distribution within a Rectangular Bagasse Layer Undergoing Drying. Drying Technology. Vol. 2. No 6. pp 749–758.

[26] Wang N. et Brennan J. G. (1995). A mathematical model of simultaneous heat and moisture transfer during drying of potato. Journal of food engineering. Vol. 24. pp 47-60.

[27] Yahaya S. (2007). Modélisation des transferts de chaleur et de masse dans les aliments: Cas du séchage de la mangue. Mémoire soutenue en vue de l'obtention du diplôme de master à l'Institut International d'Ingénierie de l'Eau et de l'Environnement (2IE).